

# Synthesis, structural and electrical properties of $\text{Bi}_{1-x}\text{Dy}_x\text{FeO}_3$ multiferroic ceramics

S.K. Barbar<sup>a</sup>, S. Jangid<sup>b</sup>, M. Roy<sup>b</sup>, F.C. Chou<sup>a,\*</sup>

<sup>a</sup>Center for Condensed Matter Sciences, National Taiwan University, Taipei 10617, Taiwan

<sup>b</sup>Department of Physics, M.L. Sukhadia University, Udaipur 313001, Rajasthan, India

Received 19 October 2012; accepted 11 December 2012

Available online 22 December 2012

## Abstract

Polycrystalline ceramic samples of dysprosium ( $\text{Dy}^{3+}$ ) doped bismuth ferrite of general formula  $\text{Bi}_{1-x}\text{Dy}_x\text{FeO}_3$  ( $x=0.00, 0.01, 0.05$  and  $0.1$ ) have been prepared by standard solid state reaction method. Powder X-ray diffraction (XRD) analysis reveals that all the samples crystallize in the rhombohedral structure with noncentrosymmetric  $R3c$  space group. The refined lattice parameters decrease with the increase of Dy concentration within the same structure symmetry. The bond lengths among atoms for all the compounds were calculated by the Rietveld analysis. The frequency and temperature dependent dielectric constants (real and imaginary parts) have been measured. The real part of dielectric constant reveals that the Neel temperature decreases with the increase of Dy-substitution down to  $\sim 200^\circ\text{C}$  for 10% substitution to the Bi site.

© 2012 Elsevier Ltd and Techna Group S.r.l. All rights reserved.

**Keywords:** C. Dielectric properties; Ceramics; Multiferroic; X-ray diffraction

## 1. Introduction

A significant interest has been generated in multiferroic materials because of the co-existence of ferroelectric and ferromagnetic properties [1]. The coupling between the magnetic moment domain and ferroelectric domain can be utilized via the magnetoelectric (M.E.) effect [2,3]. This can be realised for application in non-volatile memory where information may be recorded by controlling the direction of the electric polarization by an applied magnetic field and vice versa. However, the existence of ferroelectric and ferromagnetism is usually mutually exclusive because they require empty and partially filled transition metal orbital respectively [4]. Although multiferroics materials are less in nature due to their simultaneous ferroelectric and ferromagnetic behavior, some Bi-based materials such as  $\text{BiFeO}_3$  (BFO),  $\text{BiCrO}_3$  and  $\text{BiMnO}_3$  are quite promising still [5–7]. Among these,  $\text{BiFeO}_3$  is known to be the only material that exhibits a rhombohedrally distorted perovskite structure with space group  $R3c$  or  $C_{3v}^6$  [8]. This

compound (BFO) undergoes a displacement type ferroelectric ordering at  $T_C \sim 830^\circ\text{C}$  and the canted spins align antiferromagnetically below  $T_N \sim 370^\circ\text{C}$  [9]. Khomchenko et al. studied the room temperature crystal structure and ferroelectric properties of rare earth (Sm, Gd) doped BFO [10]. It has been observed that the bismuth based ferroelectrics such as  $\text{Bi}_4\text{Ti}_3\text{O}_{12}$  and  $\text{SrBi}_2\text{Ta}_2\text{O}_9$ , doping of lanthanum (La) was effective to enhance the insulating and ferroelectric properties because of the reduced oxygen vacancy by the stabilized oxygen octahedron [11–13]. The lanthanum (La) promotes changes in structure and dielectric/ferroelectric properties that improve leakage current density and retention free characteristics [14]. Petrov et al. measured the microwave dielectric response of La and Dy-substituted thin films but failed to state the exact value of dielectric constant and dielectric loss [15]. Uniyal and Yadav [16] concluded that there is no systematic change in dielectric constant and Neel temperature with up to 10% substitution of Dy-ion. Xu et al. observed the weak ferromagnetism in the Dy-substituted powder prepared via the sol–gel method [17]. Our primary goal is to prepare defect-free and homogenous pristine and substituted compounds so that the materials could be exploited for

\*Corresponding author.

E-mail address: [fcchou@ntu.edu.tw](mailto:fcchou@ntu.edu.tw) (F.C. Chou).

practical applications. Current report explores the impact of Dy substitution to the Bi site of  $\text{BiFeO}_3$  for the purpose of modifying the dielectric properties of pristine  $\text{BiFeO}_3$ .

## 2. Experimental

Polycrystalline samples of  $\text{Bi}_{1-x}\text{Dy}_x\text{FeO}_3$  ( $x=0.00, 0.01, 0.05$  and  $0.1$ ) have been prepared using a conventional high temperature solid state reaction technique under controlled condition of time and temperature. Stoichiometric proportions of high purity (99.99%) powders of  $\text{Bi}_2\text{O}_3$ ,  $\text{Fe}_2\text{O}_3$  and  $\text{Dy}_2\text{O}_3$  (with excess of 2 mol%,  $\text{Bi}_2\text{O}_3$ ) were mixed thoroughly and fired in the air at  $600^\circ\text{C}$  for 5 h. The pre-heated powders were well ground and calcined at  $700^\circ\text{C}$  for 5 h with intermediate grindings and then pressed into pellets and sintered at  $880^\circ\text{C}$  for 5 min. The structure and phase purity of the samples were checked by powder X-ray diffraction (XRD). The XRD patterns were obtained from Rigaku X-ray diffractometer using  $\text{CuK}\alpha$  radiation and nickel filter in a wide scanning range of  $2\theta$  from  $10$ – $90^\circ$  with a scanning rate of  $2^\circ/\text{min}$  at

room temperature. Rietveld refinement of the room temperature X-ray powder diffraction pattern was performed with the program Fullprof [18]. A pseudo-voigt function convoluted with an axial divergence asymmetry function was used to model the peak profile. The dielectric constant ( $\epsilon'$ ) and dissipation factor ( $\epsilon''$ ) were measured as a function of frequency (100 Hz–1 MHz) between 300 K and 643 using 3532-50 LCR HiTester. The dielectric measurements were performed on the circular dish-shaped (10 mm diameter and 1 mm thickness) samples with silver paint coated on two sides as the electrodes.

## 3. Results and discussion

The Rietveld refinement results of room temperature X-ray diffraction (XRD) data for the samples  $\text{Bi}_{1-x}\text{Dy}_x\text{FeO}_3$  ( $x=0.00, 0.01, 0.05$  and  $0.1$ ) are shown in Fig. 1(a–d). The XRD pattern of the pristine compound ( $x=0.00$ ) is matched well with the standard data file JCPDS#20-0169 except two to three minor low intensity impurity peaks at  $2\theta=14.62^\circ, 33.03^\circ, 33.69^\circ$  and  $46.92^\circ$  detected in Rietveld

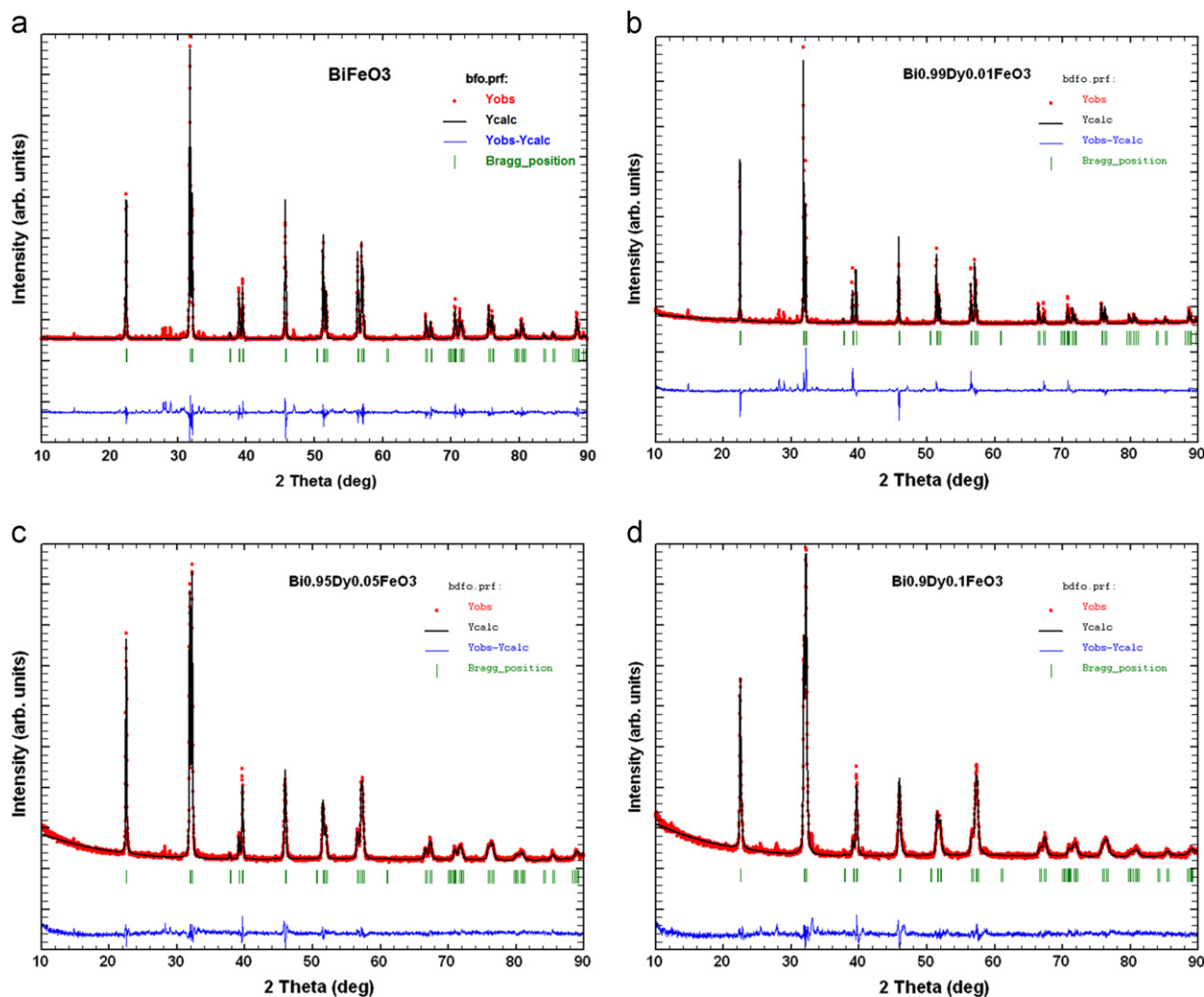


Fig. 1. (a) Rietveld refined profile of  $\text{Bi}_{1-x}\text{Dy}_x\text{FeO}_3$  ( $x=0.00$ ), (b) Rietveld refined profile of  $\text{Bi}_{1-x}\text{Dy}_x\text{FeO}_3$  ( $x=0.01$ ), (c) Rietveld refined profile of  $\text{Bi}_{1-x}\text{Dy}_x\text{FeO}_3$  ( $x=0.05$ ) and (d) Rietveld refined profile of  $\text{Bi}_{1-x}\text{Dy}_x\text{FeO}_3$  ( $x=0.1$ ).

analysis. When  $\text{Bi}^{3+}$  ion is substituted with different concentrations (0.01, 0.05 and 0.1) of  $\text{Dy}^{3+}$  ion, the XRD patterns also show identical impurity peaks found in the pristine compound. It is observed that there is a small shift in peak positions for the substituted compounds but all the said compounds described with the same space group  $R3c$ . These results suggest that all the pristine and substituted compounds have the same crystal structure.

A unit cell of hexagonal system was selected and cell parameters were refined using Rietveld analysis. Bulk  $\text{BiFeO}_3$  has a rhombohedrally distorted perovskite structure in the space group  $R3c$ . In this distorted structure, the hexagonal  $[001]_h$  is equivalent to the pseudo cubic  $[111]_c$  direction, which is the three fold rotation axis of the  $R3c$  space group [19]. Both  $\text{Bi}^{3+}$  and  $\text{Fe}^{3+}$  cations are displaced from their centrosymmetric position to give rise to a permanent dipole moment required for the ferroelectric ordering. There are three atoms in the asymmetric unit of  $\text{BiFeO}_3$  occupying the Wyckoff positions of  $6a$  ( $\text{Bi}^{3+}$  and  $\text{Fe}^{3+}$ ) and  $18b$  ( $\text{O}^{2-}$ ). The tilt angle for the anti phase rotation of the oxygen octahedra is found to be  $12.2^\circ$  [20]. The Fe magnetic moments are coupled ferromagnetically within the pseudo cubic (111) planes and antiferromagnetically between the adjacent planes leading to a G-type antiferromagnetic ordering.

The Rietveld refined profile for the pristine compound ( $x=0.00$ ) is shown in Fig. 1(a). The observed and the calculated difference pattern indicates a reasonable agreement. The four low intensity impurity peaks are not fitted for  $x=0.00$  compound. These impurity peaks are identified to be coming from the  $\text{Bi}_2\text{Fe}_4\text{O}_9$  phase. Fig. 1(b) shows the Rietveld refined profile of the  $x=0.01$  (1% Dy-doped BFO) compound. The difference pattern between the observed and the calculated shows the same impurity peaks which have been observed for  $x=0.00$  compound. No other extra impurity peaks are observed in the whole range of  $2\theta$ . Further increase of Dy concentration from  $x=0.01$  (1% Dy doped BFO) to  $x=0.05$  (5% Dy doped BFO) also shows a good agreement between the observed and the calculated patterns (Fig. 1c). The impurity peaks become weaker with increasing substitution level. When Dy concentration increases from  $x=0.05$  (5% Dy doped BFO) to 0.1 (10% Dy doped BFO), the diffraction peaks ( $2\theta=33.69^\circ$  and  $46.92^\circ$ ) that correspond to  $\text{Bi}_2\text{Fe}_4\text{O}_9$  impurity phase are significantly reduced, as shown in the Rietveld refined profile for  $x=0.1$  compound (Fig. 1d). We note that the existence of Bi–Fe–O impurity phases are difficult to avoid, no matter through solid state reaction or sol–gel preparation methods [16,17]. The  $\text{Bi}_2\text{Fe}_4\text{O}_9$  impurity phase observed in all these samples are within the error limit of less than 5% and do not affect the structural and other physical properties of the title compounds. The detailed Rietveld analysis results are summarized in Table 1.

A good agreement between the observed (based on Bragg's condition i.e.  $2d \sin\theta=n\lambda$ ) and the calculated (based on refined cell parameters)  $d$ -values for all the

Table 1

Details of the Rietveld refinement of the room temperature X-ray powder diffraction pattern of  $\text{Bi}_{1-x}\text{Dy}_x\text{FeO}_3$  ( $x=0.00, 0.01, 0.05$  and  $0.1$ ).

Parameters	$x=0.00$	$x=0.01$	$x=0.05$	$x=0.1$
$a=b$ (Å)	5.5790	5.5671	5.5570	5.5556
$c$ (Å)	13.8640	13.8397	13.8072	13.8021
Unit cell vol. (Å <sup>3</sup> )	373.776	371.468	369.256	368.932
$U$	0.08528	0.02775	0.49554	1.16546
$V$	−0.08340	−0.01394	−0.22201	−0.59220
$W$	0.03112	0.00497	0.04373	0.12519
Rp	24.1	32.6	18.3	22.4
Rwp	30.7	26.2	15.9	19.2
GOF	2.8	2.3	1.5	1.7

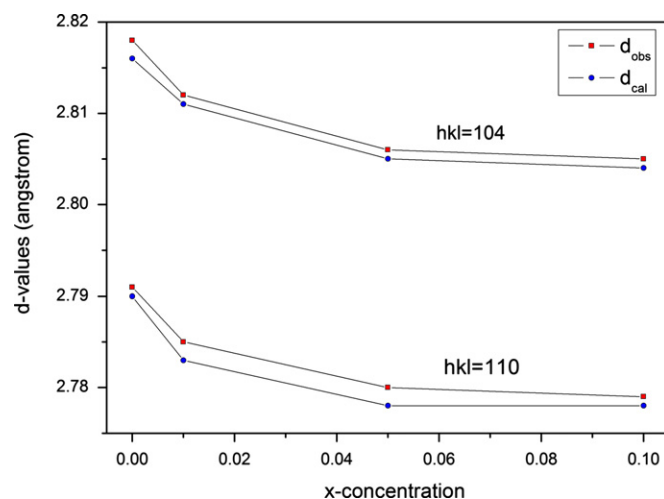


Fig. 2.  $d$ -values versus  $x$ -concentration curves of  $\text{Bi}_{1-x}\text{Dy}_x\text{FeO}_3$  ( $x=0.00, 0.01, 0.05$  and  $0.1$ ).

compounds (Fig. 2) suggests the suitability of the crystal system and unit cell parameters. On the basis of good agreement between  $d_{\text{obs}}$  and  $d_{\text{cal}}$  i.e.  $\Delta d = d_{\text{obs}} - d_{\text{cal}}$ , the final values of  $\Delta d$  are 0.001 to 0.002 for all the compounds. This data suggests that we have a reasonable fit of the experimental data in the rhombohedral system. It is also observed that the  $d$ -values decrease with the increase of Dy-substitution level. The significant change in  $d$ -values due to Dy-ion substitution may be explained in terms of the difference between ionic radii of Bi and Dy. Since, the ionic radius of Dy (0.912 Å) is smaller than that of Bi (1.03 Å), the  $d$ -spacing and the lattice parameters decrease with the increase of Dy-substitution on the Bi-site.

The bond lengths for all the compounds were calculated using the program of Bond\_Str as shown in Table 2. It is observed that the Fe–O length is significantly shorter than that of Bi–O. Table 2 also reveals that the Bi–O bond length increases with the increase of Dy substitution, which may be due to the decrease of Bi content in the compound. The octahedral bonding environment in the  $R3c$  space group is comprised of 3 long degenerate Bi–O and Fe–O bond lengths and 3 shorter degenerate bond lengths.

The variation of dielectric constant ( $\epsilon$ ) with frequency is shown in Fig. 3. It is clear that the dielectric constant decreases with the increase of frequency. The higher value of  $\epsilon$  at lower frequency is due to the presence of all types of polarizations in the compound at room temperature.

Table 2

Bond lengths between atoms of a unit cell for  $\text{Bi}_{1-x}\text{Dy}_x\text{FeO}_3$  ( $x=0.00, 0.01, 0.05$  and  $0.1$ ).

Bond type	Bond lengths (Å)			
	$x=0.00$	$x=0.01$	$x=0.05$	$x=0.1$
Bi–O	2.2997	2.4004	2.6711	2.7265
Fe–O	1.8152	1.9833	2.0038	2.0149
Dy–O	–	2.6148	2.6952	2.7793
Bi–Fe	2.5100	3.0757	3.0210	3.0147
Bi–Dy	–	1.9867	1.9330	1.6280

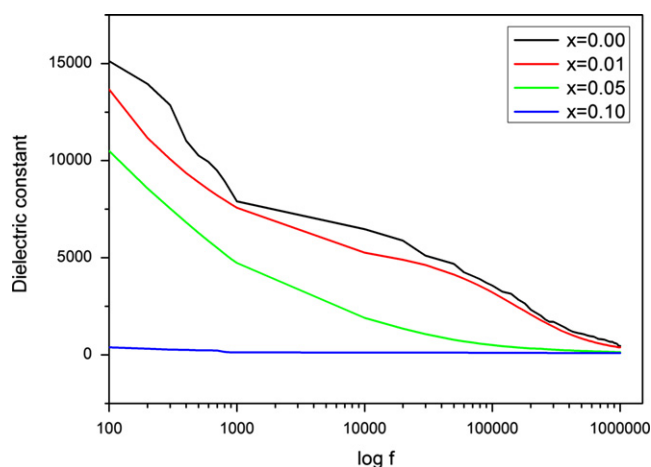


Fig. 3. Dielectric constant versus  $\log f$  curves of  $\text{Bi}_{1-x}\text{Dy}_x\text{FeO}_3$  ( $x=0.00, 0.01, 0.05$  and  $0.1$ ) at RT.

As the frequency is increased, only electronic polarization become dominates and thus the value of  $\epsilon$  decreases.

The variation of the dielectric constant of  $\text{Bi}_{1-x}\text{Dy}_x\text{FeO}_3$  compounds with temperature at frequency 10 kHz is shown in Fig. 4a. The plot reveals that the dielectric constant increases with the rise in temperature up to its maximum value ( $\epsilon_{\text{max}}$ ) at Neel temperature ( $T_N$ ) and then decreases and again increases up to the measured temperature range. It is observed that the compounds undergo a magnetic transition from antiferromagnetic to ferromagnetic at  $T_N$ . The values of Neel temperature for all compounds are shown in Table 3. It is clear from the table that the  $T_N$  shifts towards lower value as the concentration of Dy increases. This decrease in  $T_N$  with Dy concentration may be explained in terms of the variation in ionic sizes of Bi and Dy.

Fig. 4b shows the variation of tangent loss ( $\tan\delta$ ) with temperature at frequency of 10 kHz. The  $\tan\delta$  shows almost same trend as dielectric constant with no indication of any anomaly ( $T_N$ ) up to the measured temperature range. The  $\tan\delta$  decreases progressively with increasing in  $x$ -concentration. The value of  $\tan\delta$  is maximum for the pristine ( $x=0.00$ ) compound that may be due to the maximum ion migration loss taking place within the compound. Not only this, the  $\tan\delta$  is almost constant and reaching maximum after  $\sim 190^\circ\text{C}$  for all the compounds, which shows the very high dielectric loss of the BFO and its Dy substituted variations.

Table 3

Neel temperature ( $T_N$ ) values for  $\text{Bi}_{1-x}\text{Dy}_x\text{FeO}_3$  ( $x=0.00, 0.01, 0.05$  and  $0.1$ ).

$x$ -concentration	Neel temperature ( $T_N$ ) in $^\circ\text{C}$
$x=0.00$	365 (Ref. [14])
$x=0.01$	250
$x=0.05$	220
$x=0.1$	200

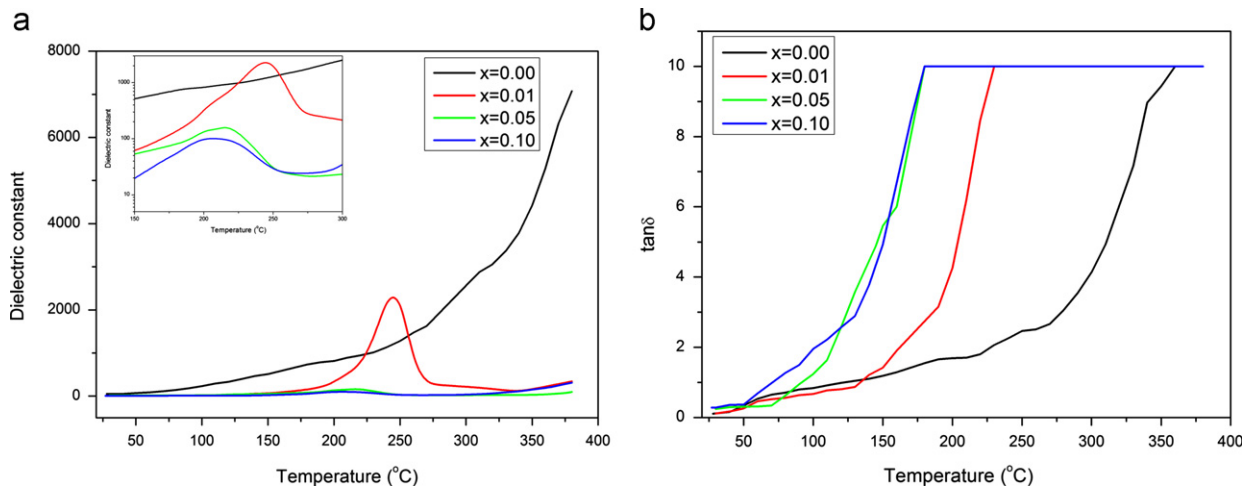


Fig. 4. (a) Dielectric constant versus temperature curves of  $\text{Bi}_{1-x}\text{Dy}_x\text{FeO}_3$  ( $x=0.00, 0.01, 0.05$  and  $0.1$ ) at 10 kHz and (b) tangent loss versus temperature curves of  $\text{Bi}_{1-x}\text{Dy}_x\text{FeO}_3$  ( $x=0.00, 0.01, 0.05$  and  $0.1$ ) at 10 kHz.

#### 4. Conclusion

Polycrystalline ceramic samples of  $\text{Bi}_{1-x}\text{Dy}_x\text{FeO}_3$  ( $x=0.00, 0.01, 0.05$  and  $0.1$ ) were prepared successfully by solid state reaction technique. X-ray diffraction analysis suggests that these compounds have the correct main phases with minor impurity phase of less than 5%. All the samples fitted with Rietveld refinement reveal the main phase has a rhombohedral structure with noncentrosymmetric space group  $R3c$ . The calculated bond lengths are in good agreement with those reported in the literature. The dielectric measurement results show that the Neel temperature ( $T_N$ ) decreases with the increase in Dy-concentration. With the reduced  $T_N$  after Dy substitution, a wider temperature range on magnetoelectric coupling control can be achieved for potential device applications.

#### Acknowledgments

The authors would like to thanks A. Hussain, S. Singh and K.S. Rao for their experimental assistance in work. FCC acknowledges support from NSC-Taiwan under Project No. NSC 100-2119-M-002-021.

#### References

- [1] N.A. Spaldin, M. Fiebig, The renaissance of magnetoelectric multiferroics, *Science* 309 (2005) 391–392.
- [2] M. Fiebig, Revival of the magnetoelectric effect, *Journal of Physics D* 38 (2005) R123–R152.
- [3] W. Prellier, M.P. Singh, P. Murugavel, The single-phase multiferroic oxides: from bulk to thin film, *Journal of Physics: Condensed Matter* 17 (2005) R803–R832.
- [4] M.M. Kumar, V.R. Palkar, K. Srinivas, S.V. Suryanarayana, Ferroelectricity in a pure  $\text{BiFeO}_3$  ceramic, *Applied Physics Letters* 76 (2000) 2764–2766.
- [5] A.H.M. Gonzalez, A.Z. Simoes, L.S. Cavalcante, E. Longo, J.A. Varela, C.S. Riccardi, Soft chemical deposition of  $\text{BiFeO}_3$  multiferroic thin films, *Applied Physics Letters* 90 (2007) 052906–052908.
- [6] D.H. Kim, H.N. Lee, M. Varela, H.M. Christen, Antiferroelectricity in multiferroic  $\text{BiCrO}_3$  epitaxial films, *Applied Physics Letters* 89 (2006) 162904–162906.
- [7] A.M. dos Santos, S. Parashar, A.R. Raju, Y.S. Zhao, A.K. Cheetham, C.N.R. Rao, Evidence for the likely occurrence of magnetoferroelectricity in the simple perovskite,  $\text{BiMnO}_3$ , *Solid State Communications* 122 (2002) 49–52.
- [8] G.A. Smolenskii, I.E. Chupis, Ferroelectromagnets, *Soviet Physics Uspekhi* 25 (1982) 475–493.
- [9] J. Wang, J.B. Neaton, H. Zheng, V. Nagarjun, S.B. Ogale, B. Liu, D. Viehland, V. Vaithyanathan, D.G. Schlom, U.V. Waghmare, N.A. Spaldin, K.M. Rabe, M. Wuttig, R. Ramesh, Epitaxial  $\text{BiFeO}_3$  multiferroic thin film heterostructures, *Science* 299 (2003) 1719–1722.
- [10] V.A. Khomchenko, J.A. Paixão, D.A. Kiselev, A.L. Kholkin, Intermediate structural phases in rare-earth substituted  $\text{BiFeO}_3$ , *Materials Research Bulletin* 45 (2010) 416–419.
- [11] J.K. Lee, C.H. Kim, H.S. Suh, K.S. Hong, Correlation between internal stress and ferroelectric fatigue in  $\text{Bi}_{4-x}\text{La}_x\text{Ti}_3\text{O}_{12}$  thin films, *Applied Physics Letters* 80 (2002) 3593–3595.
- [12] Y.Y. Yao, C.H. Song, P. Bao, D. Su, X.M. Liu, J.S. Zhu, Y.N. Wang, Doping effect on the dielectric property in bismuth titanate, *Journal of Applied Physics* 95 (2004) 3126–3130.
- [13] Y. Zhong, G. Hu, T.A. Tang, Preparation and ferroelectric properties of lanthanum modified  $\text{Sr}_{0.8}\text{Bi}_{2.2}\text{Ta}_2\text{O}_9$  thin films, *Japanese Journal of Applied Physics* 42 (2003) 7424–7427.
- [14] S. Jangid, S.K. Barbar, Indu Bala, M. Roy, Structural, thermal, electrical and magnetic properties of pure and 50% La doped  $\text{BiFeO}_3$  ceramics, *Physica B: Condensed Matter* 407 (2012) 3694–3699.
- [15] P.K. Petrov, V.R. Palkar, A.K. Tagantsev, H.I. Chien, K. Prashanthi, A.K. Axelsson, S. Bhattacharya, N.McN Alford, Dielectric properties characterization of La and Dy doped  $\text{BiFeO}_3$  thin films, *Journal of Materials Research* 22 (2007) 2179–2184.
- [16] P. Uniyal, K.L. Yadav, Observation of the room temperature magnetoelectric effect in Dy doped  $\text{BiFeO}_3$ , *Journal of Physics: Condensed Matter* 21 (2009) 012205–012208.
- [17] J.M. Xu, G.M. Wang, H.X. Wang, D.F. Ding, Y. He, Synthesis and weak ferromagnetism of Dy-doped  $\text{BiFeO}_3$  powders, *Materials Letters* 63 (2009) 855–857.
- [18] J. Rodriguez-Carvajal, Recent developments of the program fullprof, in commission on powder diffraction, *IUCr Newsletters* 26 (2001) 12–19.
- [19] C. Michel, J.M. Moreau, G.D. Achenbach, R. Gerson, W.J. James, The atomic structure of  $\text{BiFeO}_3$ , *Solid State Communications* 7 (1969) 701–704.
- [20] P. Fischer, M. Polomska, I. Sosnowska, M. Szymanski, Temperature dependence of the crystal and magnetic structures of  $\text{BiFeO}_3$ , *Journal of Physics C: Solid State Physics* 13 (1980) 1931–1940.